

Hydrodynamic and hydromagnetic energy spectra from large eddy simulations

Nils Erland L. Haugen^{a)}

Department of Physics, The Norwegian University of Science and Technology, Høyiskoleringen 5,
N-7034 Trondheim, Norway and SINTEF Energy Research, Kolbjørn Hejes Vei 1A,
N-7465 Trondheim, Norway

Axel Brandenburg^{b)}

NORDITA, Blegdamsvej 17, DK-2100 Copenhagen Ø, Denmark

(Received 20 March 2006; accepted 19 June 2006; published online 26 July 2006)

Direct and large eddy simulations of hydrodynamic and hydromagnetic turbulence have been performed in an attempt to isolate artifacts from real and possibly asymptotic features in the energy spectra. It is shown that in a hydrodynamic turbulence simulation with a Smagorinsky subgrid scale model using 512^3 mesh points, two important features of the 4096^3 simulation on the Earth simulator [Y. Kaneda *et al.*, Phys. Fluids **15**, L21 (2003)] are reproduced: a $k^{-0.1}$ correction to the inertial range with a $k^{-5/3}$ Kolmogorov slope and the form of the bottleneck just before the dissipative subrange. Furthermore, it is shown that, while a Smagorinsky-type model for the induction equation causes an artificial and unacceptable reduction in the dynamo efficiency, hyper-resistivity yields good agreement with direct simulations. In the large-scale part of the inertial range, an excess of the spectral magnetic energy over the spectral kinetic energy is confirmed. However, a trend toward spectral equipartition at smaller scales in the inertial range can be identified. With magnetic fields, no explicit bottleneck effect is seen. © 2006 American Institute of Physics. [DOI: 10.1063/1.222399]

I. INTRODUCTION

In astrophysical magnetohydrodynamic (MHD) turbulence, e.g., in stars, accretion disks, the interstellar medium, and the intergalactic medium, the magnetic and fluid Reynolds numbers are very large. It is therefore of great interest to perform simulations with as large a Reynolds number as possible. However, the goal of reaching astrophysical values of the magnetic Reynolds numbers is still far out of reach. The best we can hope for, therefore, is to find asymptotic trends such that one can extrapolate into the very large Reynolds number regime. However, even that is not really possible as the following estimate shows. As a rule of thumb, for a purely hydrodynamical simulation one needs at least an order of magnitude to resolve the dissipative subrange, one order of magnitude for the bottleneck (a shallower spectrum just before the dissipative subrange), and almost an order of magnitude for the forcing to become isotropic. This leaves basically nothing for the inertial range—even for simulations with 1024^3 mesh points. It is therefore only with simulations as big as 4096^3 mesh points¹ that one begins to see an inertial range.

In MHD turbulence without imposed field, i.e., when the field is self-consistently generated by dynamo action, the magnetic energy spectrum peaks at a wave number that is larger by a certain factor than the wave number of the kinetic energy spectrum.² This factor has been related to the value of the critical magnetic Reynolds number for dynamo action,

$\text{Re}_{M,\text{crit}}$. Specifically, $k_{\text{mag}} \approx k_{\text{kin}} \text{Re}_{M,\text{crit}}^{1/2}$ has been suggested,³ where k_{mag} and k_{kin} are the wave numbers of the peaks of the magnetic and kinetic energy spectra, respectively, and $\text{Re}_{M,\text{crit}} \approx 35$.⁴ This leads to the conclusion that in MHD turbulence one needs an even larger Reynolds number than for purely hydrodynamical turbulence in order to have a chance to see an inertial range.

What has been found so far is that there is a certain range, $k_{\text{mag}} \leq k \leq k_d$, where the spectral magnetic energy exceeds the spectral kinetic energy,^{2,4} i.e., there is spectral superequipartition. While spectral superequipartition is not *a priori* implausible, it is curious that this has not been seen in simulations with an imposed field. Such simulations with imposed field have recently been performed^{5–7} to verify the Goldreich-Sridhar theory of MHD turbulence.⁸ More systematic studies of the resulting energy spectra as a function of the imposed field strength have been carried out,⁹ and it was found that there is spectral equipartition only when the imposed field, B_0 , is of equipartition strength, i.e., $B_0^2 \sim \mu_0 \rho_0 u_{\text{rms}}^2$, where μ_0 is the vacuum permeability, ρ_0 is the mean density, and u_{rms} is the rms velocity. If B_0 is larger, the magnetic spectrum is always in subequipartition.

The case of an imposed field is usually thought to be representative of the conditions deep in the inertial range. Thus, the observed superequipartition does seem to be in conflict with this result. This is also supported by the well known fact that in the solar wind, kinetic and magnetic energy spectra follow a power law with an $-5/3$ exponent over several decades.¹⁰ In this work, we want to elucidate this puzzle by comparing direct simulations with simulations using hyperviscosity and hyper-resistivity, as well as Smagor-

^{a)}Electronic mail: Nils.E.Haugen@sintef.no

^{b)}Electronic mail: brandenb@nordita.dk

insky subgrid scale (SGS) modeling, in order to imitate larger Reynolds numbers. For recent comparisons between direct and Smagorinsky SGS simulations; see Refs. 11–14, where also decaying turbulence is considered, albeit only at a resolution of 64^3 mesh points. This was too small to discuss the shape of the energy spectra. Recent simulations using hyperviscosity have shown that at large enough resolution (512^3 mesh points), the same $k^{-0.1}$ correction to the Kolmogorov $k^{5/3}$ inertial range spectrum is seen¹⁵ as in the 4096^3 mesh points direct simulations of Kaneda *et al.*¹ In the present paper, we compare these two simulations also with new Smagorinsky SGS models.

We need to emphasize that throughout this paper, we only deal with the case of “nonhelical” turbulence, i.e., $|\langle \mathbf{u} \cdot \nabla \times \mathbf{u} \rangle|$ is negligible (or small compared with $k_f \langle u^2 \rangle$, where k_f is the typical forcing wave number). In some sense, the case of finite helicity may be regarded as more typical.¹⁶ However, with helicity there is a whole range of new problems that need to be addressed. For example, when using hyper-resistivity the magnetic field would saturate at an artificially enhanced value when there is helicity.¹⁷ These helicity effects are now fairly well understood (see Ref. 18 for a review), but in the present paper we discard these complications.

II. METHOD

We solve the compressible nonideal MHD equations,

$$\frac{D\mathbf{u}}{Dt} = -\frac{1}{\rho} \nabla p + \frac{\mathbf{J} \times \mathbf{B}}{\rho} + \mathbf{f} + \mathbf{F}_{\text{visc}}, \quad (1)$$

where $D/Dt = \partial/\partial t + \mathbf{u} \cdot \nabla$ is the advective derivative, p is the pressure, ρ is the density, \mathbf{f} is an isotropic random nonhelical forcing function with power in a narrow band of wave numbers, \mathbf{B} is the magnetic field, $\mathbf{J} = \nabla \times \mathbf{B} / \mu_0$ is the current density, and \mathbf{F}_{visc} is the viscous force (see below). We consider an isothermal gas with constant sound speed c_s , so that the pressure is given by $p = c_s^2 \rho$ and $\rho^{-1} \nabla p = c_s^2 \nabla \ln \rho$. The density obeys the continuity equation,

$$\frac{D \ln \rho}{Dt} = -\nabla \cdot \mathbf{u}. \quad (2)$$

The induction equation is solved in terms of the magnetic vector potential \mathbf{A} ,

$$\frac{\partial \mathbf{A}}{\partial t} = \mathbf{u} \times \mathbf{B} - \mathbf{E}_{\text{res}}, \quad (3)$$

where $\mathbf{B} = \nabla \times \mathbf{A}$ is the magnetic flux density and \mathbf{E}_{res} is the electric field due to resistive effects (see below).

In the following, different combinations of expressions for \mathbf{F}_{visc} and \mathbf{E}_{res} have been explored. In all simulations, these expressions are of the general form

$$\mathbf{F}_{\text{visc}} = \frac{1}{\rho} \nabla \cdot (2\rho\nu\mathbf{S}), \quad \mathbf{E}_{\text{res}} = \eta\mu_0\mathbf{J}, \quad (4)$$

where

$$\mathbf{S}_{ij} = \frac{1}{2} \left(\frac{\partial u_i}{\partial x_j} + \frac{\partial u_j}{\partial x_i} - \frac{2}{3} \delta_{ij} \nabla \cdot \mathbf{u} \right) \quad (5)$$

is the traceless rate of strain tensor. In a direct simulation, we simply use constant values of ν and η , i.e.,

$$\nu = \nu_0, \quad \eta = \eta_0 \quad (\text{direct}). \quad (6)$$

In the case of a Smagorinsky SGS model, we use $\nu = \nu_S$ and $\eta = \eta_S$ (without constant contributions) where

$$\nu_S = (C_K \Delta)^2 \sqrt{2\mathbf{S}^2}, \quad \eta_S = (C_M \Delta)^2 \sqrt{\mathbf{J}^2} (\text{Smagorinsky}), \quad (7)$$

where C_K is the Smagorinsky constant, C_M is the magnetic Smagorinsky constant, and Δ is the filter size, which we have set equal to the mesh size. This version of the magnetic Smagorinsky SGS model has been studied earlier; see, e.g., Ref. 11. We choose $C_K = 0.2$, but we vary the value of C_M . In simulations with hyperviscosity, we replace

$$\rho\nu\mathbf{S} \rightarrow \rho_0\nu_3\nabla^4\mathbf{S}, \quad \eta\mathbf{J} \rightarrow \eta_3\nabla^4\mathbf{J} \quad (\text{hyper}) \quad (8)$$

in Eq. (4), and use constant coefficients, referred to as $\nu = \nu_3$ and $\eta = \eta_3$. Following Ref. 15, we use constant *dynamical* hyperviscosity, $\rho_0\nu_3 = \text{const}$, in which case a positive viscous heating term can be defined.

In the present work, we only consider cases with small Mach number. Compressibility effects are therefore unimportant,¹⁹ and the continuity equation (2) can therefore be solved without additional subgrid scale terms. We note, however, that by defining suitable averages (Favre filtering; see Ref. 20), the continuity does formally retain its original form. Likewise, in strongly compressible flows a turbulent bulk viscosity will be important for smearing out shocks; see, e.g., Ref. 21. Again, this is neglected, because we are only interested here in nearly incompressible flows.

It is customary to quote Reynolds numbers based on the Taylor microscale $\lambda = \sqrt{5}u_{\text{rms}}/\omega_{\text{rms}}$, where ω_{rms} is the rms vorticity, and on the one-dimensional velocity dispersion u_{1D} , where $u_{1D}^2 = u_{\text{rms}}^2/3$. Hence, we define the fluid and magnetic Reynolds numbers for a direct numerical simulation as

$$\text{Re}_\lambda = \frac{u_{1D}\lambda}{\nu}, \quad \text{Re}_M = \frac{u_{1D}\lambda}{\eta}, \quad (9)$$

respectively. Their ratio is the magnetic Prandtl number, $\text{Pr}_M = \nu/\eta = \text{Re}_M/\text{Re}$, which is unity for all runs. For the hyperviscous and Smagorinsky cases, we define the Taylor microscale Reynolds number, in analogy to earlier work,¹⁵ as

$$\text{Re}_\lambda = \text{Re}_{\lambda,0} \left(\frac{k_{d,\text{eff}}}{k_f} \right)^{2/3}, \quad (10)$$

where we have defined the effective Kolmogorov wave number, $k_{d,\text{eff}}$, whose value is found empirically by making the inertial ranges of the spectra overlap as best as possible, and $\text{Re}_{\lambda,0}$ is a calibration parameter. In an earlier paper,¹⁵ the calibration parameter was found to be $\text{Re}_{\lambda,0} \approx 7.5$, which is also the value chosen here.

We use nondimensional quantities by measuring length in units of $1/k_1$ (where $k_1 = 2\pi/L$ is the smallest wave number in the box of size L), speed in units of the isothermal

sound speed c_s , density in units of the initially uniform value $\rho = \rho_0$, and magnetic field in units of $(\mu_0 \rho_0 c_s^2)^{1/2}$.

We use periodic boundary conditions in all three directions for all variables. This implies that the mass in the box is conserved, i.e., $\langle \rho \rangle = \rho_0$, where angular brackets denote volume averages. We adopt a forcing function f of the form

$$f(\mathbf{x}, t) = \Re\{N f_{k(t)} \exp[i\mathbf{k}(t) \cdot \mathbf{x} + i\phi(t)]\}, \quad (11)$$

where \mathbf{x} is the position vector, and \Re indicates the real part. The wave vector $\mathbf{k}(t)$ and the random phase $-\pi < \phi(t) \leq \pi$ change at every time step, so $f(\mathbf{x}, t)$ is δ -correlated in time. For the time-integrated forcing function to be independent of the length of the time step δt , the normalization N has to be proportional to $\delta t^{-1/2}$. On dimensional grounds, it is chosen to be $N = f_0 c_s (|\mathbf{k}| c_s / \delta t)^{1/2}$, where f_0 is a nondimensional forcing amplitude. The value of the coefficient f_0 is chosen such that the maximum Mach number stays below about 0.2. Empirically, this is achieved by taking $f_0 = 0.02$ for all runs discussed below.

At each time step, we select randomly one of many possible wave vectors in a certain range around a given forcing wave number. The average wave number is referred to as k_f . We force the system with nonhelical transversal waves,

$$f_{\mathbf{k}} = (\mathbf{k} \times \mathbf{e}) / \sqrt{k^2 - (\mathbf{k} \cdot \mathbf{e})^2}, \quad (12)$$

where \mathbf{e} is an arbitrary unit vector that is real and not aligned with \mathbf{k} ; note that $|\mathbf{f}_{\mathbf{k}}|^2 = 1$. For all simulations we use the PENCIL CODE (<http://www.nordita.dk/software/pencil-code>), which is a grid-based high-order code (sixth order in space and third order in time) for solving the compressible hydro-magnetic equations.

III. RESULTS

In an earlier paper,¹⁵ we showed that although hyperviscosity does cause an artificially enhanced bottleneck effect in purely hydrodynamic turbulence, it does not affect the inertial range if the resolution is large enough. Instead, hyperviscous simulations with 512^3 mesh points reproduce the $k^{-0.1}$ correction with wave number k . This was first found by Kaneda *et al.*¹ We begin by comparing these results with simulations where Smagorinsky SGS viscosity is used.

A. Hydrodynamic turbulence

In Fig. 1, we compare kinetic energy spectra of runs using ordinary viscosity (4096^3 mesh points, solid line) by Kaneda *et al.*¹ with runs using Smagorinsky viscosity (512^3 mesh points, dashed line) and runs using hyperviscosity (512^3 mesh points, dash-dotted line). Since the simulation with 4096^3 mesh points and ordinary viscosity is the largest direct simulation to date, we use it as our benchmark. The spectra for the runs with hyperviscosity and Smagorinsky viscosity have been scaled by empirically determined factors 1.1 and 0.95, respectively, so as to make the spectra overlap within the inertial range. However, these scaling factors are still well within the range over which the spectra fluctuate in time.

We see that at all scales (including those of the bottleneck) the simulation with Smagorinsky SGS modeling is sur-

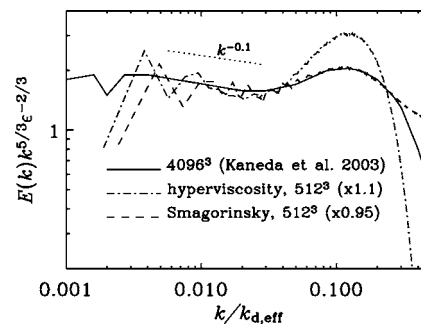


FIG. 1. Comparison of energy spectra of the 4096^3 mesh points run¹ (solid line) and 512^3 mesh points runs with hyperviscosity (dash-dotted line) and Smagorinsky viscosity (dashed line). (In the hyperviscous simulation, we use $\nu = \nu_3 = 5 \times 10^{-13}$.) The Taylor microscale Reynolds number of the Kaneda simulation is 1201, while the hyperviscous simulation of Ref. 15 has an approximate Taylor microscale Reynolds number of $340 < Re_\lambda < 730$. For the Smagorinsky simulation, the value of Re_λ is slightly smaller.

prisingly similar to the benchmark result. Furthermore, we see that at large scales and in the inertial range the run with hyperviscosity agrees well with the benchmark result. The bottleneck is, however, greatly exaggerated in height, even though the width is the same.¹⁵

Most important is perhaps the $k^{-0.1}$ correction to the usual $k^{-5/3}$ inertial range scaling. The same correction is seen in all three simulations. The $k^{-0.1}$ correction is stronger than the usual intermittency correction predicted by the She-Leveque model,²² which would only predict a $k^{-0.03}$ correction. This strong correction may be an artifact of the absence of a well resolved subinertial range.²³ This would be in some ways just opposite to the emergence of a shallower spectrum near the dissipative cutoff wave number if the dissipative subrange is not well resolved.²⁴

The only major discrepancy between the Smagorinsky and direct simulations is the lack of a sharp decline of the spectral energy toward the right of the bottleneck. In order to understand this difference, we must first of all recall that our Smagorinsky simulation did not have any explicit (constant) component at all ($\nu_0 = 0$). Therefore, if the Smagorinsky model were a perfect subgrid scale model, it would represent the infinite Reynolds number case. The bottleneck would then be far to the right and outside the graph, so one would only have a pure Kolmogorov spectrum. The reason for the bottleneck in the Smagorinsky case is therefore related to the fact that we are still working here with an ordinary diffusion operator using just a variable viscosity coefficient. Therefore, the standard explanation for the bottleneck still applies; it is caused by strongly nonlocal interactions in wave-number space, corresponding to wave vectors forming strongly elongated triangles. Close to the viscous cutoff wave number, these interactions prevent the disposal of energy from the end of the inertial range, which then causes the pileup of energy near the dissipation wave number.²⁴ The same argument also applies to the current case of Smagorinsky viscosity. In conclusion, the reason for the discrepancy between direct and Smagorinsky simulations to the right of the bottleneck is that the Smagorinsky model tries to maintain pure

TABLE I. Summary of the most important runs. The meaning of the entries in the columns for ν and η depends on the entry for “Method,” as explained in the text. In the Smagorinsky cases, ordinary viscosity is neglected, i.e., $\nu=0$. Except for Method O, the resulting values of $k_{d,eff}$, and hence also of Re_λ , are uncertain within $\sim 40\%$.

Run	Res.	Method	ν	η	$k_{d,eff}$	Re_λ
A	1024^3	O	8×10^{-5}	8×10^{-5}	143	200 ^a
B1	128^3	II	0	1×10^{-9}	180	180
B2	256^3	II	0	3×10^{-11}	330	270
B3	512^3	II	0	5×10^{-13}	700	450
C1	128^3	III	1×10^{-9}	1×10^{-9}	180	180
C2	256^3	III	3×10^{-11}	3×10^{-11}	330	270
C3	512^3	III	5×10^{-13}	5×10^{-13}	700	450

^aNote that in Ref. 25, the value of Re_λ was based on the three-dimensional velocity dispersion, so the nonmagnetic equivalent of run A was quoted with $Re_\lambda=350$.

Kolmogorov scaling everywhere, but fails to do so just before the cutoff wave number imposed by the finite mesh resolution.

B. Hydromagnetic turbulence

For the MHD case, we use a 1024^3 mesh points simulation with ordinary viscosity as our benchmark.² We compare with the SGS model where Smagorinsky schemes are used both for the velocity and the magnetic fields. In the following, we refer to this as Method I. We also compare with cases where we use hyper-resistivity. In the momentum equation, we use either the usual Smagorinsky SGS model, which is referred to as Method II, or we use hyperviscosity (Method III). The results of these three methods are compared with those of direct simulations (Method O). In summary, the different methods considered here are

Method I: ν_S and η_S (full Smagorinsky),

Method II: ν_S and η_3 (Smagorinsky/hyper),

Method III: ν_3 and η_3 (full hyper),

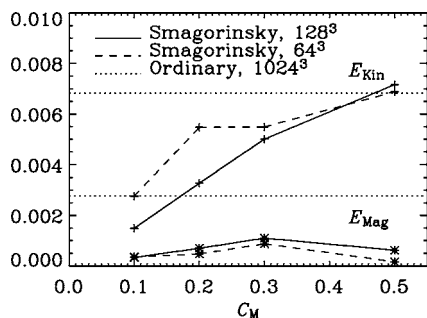


FIG. 2. Total magnetic and kinetic energies for runs with 128^3 (solid line) and 64^3 (dashed line) mesh points and Smagorinsky diffusion and resistivity (Method I) compared with a direct simulation with 1024^3 mesh points (Method O, horizontal dotted lines). Note the lack of convergence for any value of C_M .

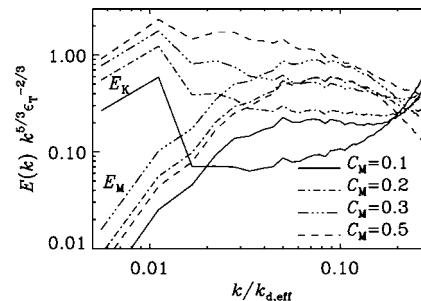


FIG. 3. Comparison of magnetic and kinetic energy spectra of runs using Method I with 128^3 mesh points and various values of C_M .

Method O: ν_0 and η_0 (benchmark).

We have listed the relevant runs in Table I.

In Fig. 2, we show that the agreement between the results of Method I and the benchmark is poor. The dynamo-generated magnetic energy remains far below the benchmark target. The largest value of the magnetic energy is reached for $C_M=0.3$, but even then it is only about 30% of the target value.

In order to understand the reason for the poor performance of the magnetic Smagorinsky model (Method I), we plot in Fig. 3 kinetic and magnetic energy spectra for various values of C_M . Clearly, for $C_M \leq 0.3$ both kinetic and magnetic spectra diverge toward large wave numbers. This shows that this model becomes unphysical and cannot be used for too small values of C_M . For $C_M=0.5$, on the other hand, magnetic and kinetic spectra fall off at large wave numbers. However, the effective resistivity of the magnetic Smagorinsky scheme is apparently too large for $C_M=0.5$, so that the dynamo is suppressed. The poor performance of this model is not too surprising if one recalls that it is a rather crude method in that it deals with the small scales only in a diffusive manner. We also note that the Smagorinsky SGS model has, to our knowledge, never before been tested in the context of dynamo action. We conclude that using the Smagorinsky SGS model for the magnetic field does not give satisfactory results. Therefore, from now on, we discard it as inappropriate for our purpose.

We see from Fig. 4 that the compensated spectra with

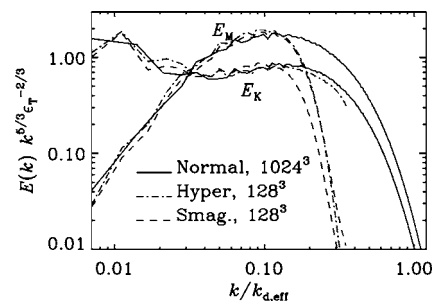


FIG. 4. Comparison of magnetic and kinetic energy spectra of runs with 1024^3 mesh points and normal diffusion (run A, solid line) with 128^3 mesh points and hyperdiffusion (run C1, dash-dotted line), and with 128^3 mesh points and Smagorinsky viscosity and hyper-resistivity (run B1, dashed line). Note that both the magnetic and kinetic energy spectra for the three runs are very similar for $k/k_d < 0.1$.

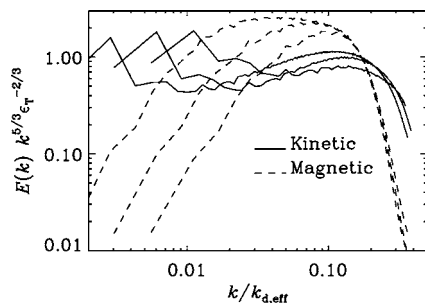


FIG. 5. Magnetic and kinetic energy spectra for runs with 128^3 (run B1), 256^3 (run B2), and 512^3 (run B3) mesh points where all of them use Smagorinsky viscosity and hyper-resistivity (Method II). Note the approach of the kinetic energy spectra toward the magnetic energy spectra at a point that is well before entering the bottleneck and the dissipative subrange.

only 128^3 mesh points, using Methods II and III, match the benchmark quite well at all scales down to the dissipative scale. We have compensated the energy spectra by $k^{5/3} \epsilon_T^{-2/3}$, such that a Kolmogorov-like spectrum would appear flat. Here $\epsilon_T = \epsilon_K + \epsilon_M$, where ϵ_K and ϵ_M are the kinetic and magnetic dissipation rates, respectively. The kinetic energy spectrum of the 1024^3 run has, however, been multiplied by 1.3 in order to make all spectra overlap. We believe the shift is due to the fact that the 1024^3 run has not been run for very long, and the average dissipation rate, ϵ_T , has not yet fully converged, even though the slope converges generally much quicker. From the general agreement between the three runs shown in Fig. 4 we conclude that, for our purpose, Methods II and III give useful results.

In Fig. 5, we compare compensated spectra for three simulations that all use Smagorinsky viscosity and hyper-resistivity, but have different Reynolds numbers. We see that, unlike the purely hydrodynamic case, the dissipative subranges do not collapse onto the same functional form for different Reynolds numbers. On the other hand, for purely hydrodynamical simulations¹⁵ the dissipative subranges collapse very well onto the same functional form and the inertial range simply becomes longer for larger Reynolds numbers. Furthermore, in Fig 1 of Ref. 15 we see that the bottleneck is similar and constant for all Reynolds numbers. Again, in the MHD simulation we see nothing similar.

In Fig. 6, we have shown the same as in Fig. 5, but using hyperviscosity instead of Smagorinsky viscosity. We clearly see that the tendency is the same in both figures. Since the

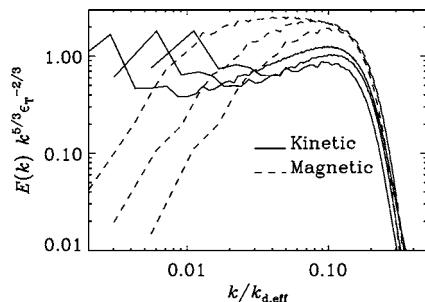


FIG. 6. Magnetic and kinetic energy spectra for runs with 128^3 (run C1), 256^3 (run C2), and 512^3 (run C3) mesh points where all of them use hyperviscosity and hyper-resistivity (Method III).

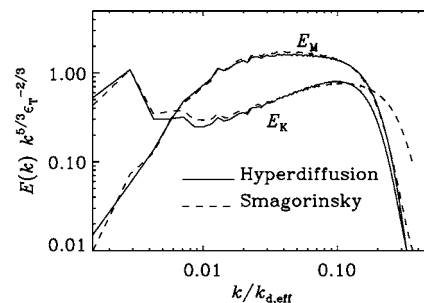


FIG. 7. Magnetic and kinetic energy spectra for runs with 512^3 mesh points and hyperviscosity and hyper-resistivity (run C3, solid line) and Smagorinsky viscosity and hyper-resistivity (run B3, dashed line). Note the mutual approach of kinetic and magnetic energy spectra before entering the dissipative subrange.

bottleneck effect is quite different for pure hydrodynamical simulations with Smagorinsky viscosity and with hyperviscosity (see Fig. 1), it is reasonable to assume that the tendency we see is robust and not due to the specific modeling applied, but that it is a physical effect.

Finally, we compare in Fig. 7 spectra of Smagorinsky and hyperviscous simulations using the highest available resolution of 512^3 mesh points. Again, note that the spectra for hyperviscous simulations and those with Smagorinsky SGS modeling are almost identical. Furthermore, there is no range where both kinetic and magnetic energy spectra are parallel. Together with the results of Figs. 5 and 6, therefore, we conclude that we have not yet reached Reynolds numbers large enough to show an inertial range.

IV. SPECULATIONS ON ASYMPTOTICS

The direct MHD simulations of Ref. 2 have suggested the presence of a superequipartition range where $E_M(k) \sim 2.5E_K(k)$. However, the spectra still showed some weak bending, indicating that a proper inertial range has not been reached even at a resolution of 1024^3 mesh points.²⁶ The present SGS models reproduce the spectral superequipartition of magnetic over kinetic spectral energy (Fig. 7), but they also show now more clearly that the two spectra are not parallel to each other. Instead, they approach each other in such a way that the compensated kinetic energy spectrum shows a strong uprise.

One might argue that the uprise at the end of the compensated kinetic spectrum is just a strong bottleneck. This is, however, unlikely since both SGS models give the same uprise, even though in purely hydrodynamic turbulence the hyperviscosity model is known to produce a much higher bottleneck than the Smagorinsky model (Sec. III A). Furthermore, in hydrodynamic turbulence the width of the bottleneck is independent of Reynolds number, whereas in the present case it appears to become wider with increasing Reynolds number. This suggests that the uprise in the MHD case is a true large-scale feature of the spectrum, and independent of the dissipative subrange.

Next, we recall that in simulations with an imposed magnetic field, the magnetic and kinetic energy spectra are found to be in approximate equipartition only when the field

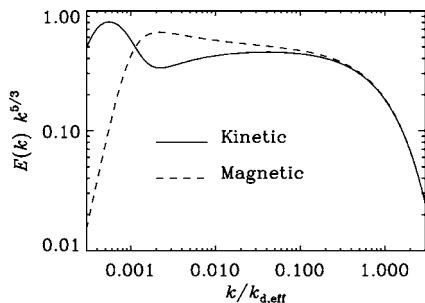


FIG. 8. Sketch of kinetic and magnetic energy spectra, following the Müller and Grappin phenomenology. Note the slight superequipartition just to the right of the peak of $E_M(k)$ and the asymptotic equipartition for large wave numbers.

strength is of the order of B_{eq} .⁹ Such simulations are thought to be representative of the small-scale end of the inertial range of any MHD simulation, even if the field is generated by a small-scale dynamo as in the present case. Assuming that this interpretation is correct, it would support our previous suggestion that the spectral superequipartition was only a nonasymptotic feature, confined to the large scales, and not a true inertial range feature. We are therefore led to believe that for much larger Reynolds numbers, the kinetic and magnetic energy spectra might converge. Qualitatively, this can be reproduced by the phenomenology proposed recently by Müller and Grappin.^{27,28} According to their theory, the total energy $E_T = E_M + E_K$ follows still the expected $k^{-5/3}$ spectrum, while the residual energy $E_R = |E_M - E_K|$ follows a $k^{-7/3}$ spectrum. In Fig. 8, we produce such an example with

$$E_T(k) = k^{-5/3} e^{-k/k_d}, \quad E_R(k) = a k^{-7/3} e^{-k/k_d}, \quad (13)$$

for $k \geq 1$ (in arbitrary units). Using the fact that in the inertial range E_M exceeds E_K by about a factor $a=2$, we reconstruct E_M and introduce an additional k^2 subinertial range, so we write

$$E_M(k) = \frac{1}{2} [E_T(k) + E_R(k)] [1 + (k/k_M)^{-11/3}], \quad (14)$$

with $k_M=5$. The kinetic energy obtained by assuming that the total energy is constant is

$$E_K(k) = [E_T(k) - E_M(k)] [1 + (k/k_K)^{-11/3}], \quad (15)$$

where we have included a different subinertial range below $k_K=1.5$. The resulting spectra shown in Fig. 8 reproduce surprisingly well the basic features suggested by our SGS simulations of Fig. 7.

In order to see how well our simulations reproduce the anticipated $k^{-7/3}$ scaling of the residual spectrum, we plot in Fig. 9 the appropriately compensated E_R spectrum. Clearly, the residual spectrum is still curved, but it remains reasonably straight within about half an order of magnitude in wave numbers.

V. CONCLUSIONS

The results of subgrid scale models should always be taken with great care. Even if their results can be trusted in one case (e.g., in the case without magnetic fields), they may

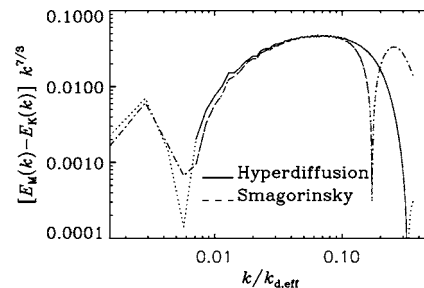


FIG. 9. Residual spectrum, $E_R = E_M - E_K$, compensated by $k^{7/3}$, for the same runs shown in Fig. 7. Negative values of $E_M - E_K$ are indicated by dotted and dash-dotted lines for hyperdiffusion and Smagorinsky runs, respectively.

not give reliable results in another case (e.g., in the presence of magnetic fields and dynamo action). However, once we begin to see detailed agreement between SGS models and direct simulations, it may be possible to use this agreement to justify the use of the SGS model in more extreme parameter regimes that are currently inaccessible to direct simulations.

In the present work, we have shown that the Smagorinsky SGS model with a resolution of 512^3 mesh points is able to reproduce the hydrodynamic turbulence spectra of a direct simulation at an almost 10 times larger resolution (Fig. 2). On the other hand, an extension of this model to the MHD case with dynamo action leads to obvious problems (the intensity of the dynamo is artificially suppressed). However, using hyper-resistivity instead of a Smagorinsky-type SGS model leads to fair agreement between the 128^3 SGS simulation and the nearly 10 times larger direct simulation (Fig. 4). Thus, having validated the SGS model at 128^3 mesh points, we may be justified in proceeding further to a resolution of 512^3 mesh points (Fig. 7). Here, a new and yet unconfirmed feature arises: a *tendency* toward spectral equipartition. This, together with the knowledge that there is spectral equipartition with imposed fields of equipartition strength,⁹ suggests a spectrum that might look like what is shown in Fig. 8.

Obviously, we will not be able to verify this result in the immediate future. Although it may soon be possible to obtain the resources necessary to do a 4096^3 MHD simulation to validate the results of Fig. 7, yet another order of magnitude in improved resolution will be necessary to test the hypothesis sketched in Fig. 8. Our results may therefore serve as a justification for using future computing resources for this type of problem.

ACKNOWLEDGMENTS

We thank the three anonymous referees for making useful suggestions that have improved the presentation of the paper. This work has been supported in part by a David Crighton Fellowship and by the Isaac Newton Institute in Cambridge, where part of this work has been carried out. We thank the Danish Center for Scientific Computing for granting time on the Horseshoe cluster, and the Norwegian High Performance Computing Consortium (NOTUR) for granting

time on the parallel computers in Trondheim (Gridur/Embla) and Bergen (Fire).

- ¹Y. Kaneda, T. Ishihara, M. Yokokawa, K. Itakura, and A. Uno, "Energy dissipation rate and energy spectrum in high resolution direct numerical simulations of turbulence in a periodic box," *Phys. Fluids* **15**, L21 (2003).
- ²N. E. L. Haugen, A. Brandenburg, and W. Dobler, "Is nonhelical hydro-magnetic turbulence peaked at small scales?" *Astrophys. J. Lett.* **597**, L141 (2003).
- ³K. Subramanian, "Can the turbulent galactic dynamo generate large scale magnetic fields?" *Mon. Not. R. Astron. Soc.* **294**, 718 (1998).
- ⁴N. E. L. Haugen, A. Brandenburg, and W. Dobler, "Simulations of non-helical hydromagnetic turbulence," *Phys. Rev. E* **70**, 016308 (2004).
- ⁵J. Cho and E. Vishniac, "The anisotropy of magnetohydrodynamic Alfvénic turbulence," *Astrophys. J.* **539**, 273 (2000).
- ⁶J. Maron and P. Goldreich, "Simulations of incompressible magnetohydrodynamic turbulence," *Astrophys. J.* **554**, 1175 (2001).
- ⁷W.-C. Müller, D. Biskamp, and R. Grappin, "Statistical anisotropy of magnetohydrodynamic turbulence," *Phys. Rev. E* **67**, 066302 (2003).
- ⁸P. Goldreich and S. Sridhar, "Toward a theory of interstellar turbulence. 2: Strong Alfvénic turbulence," *Astrophys. J.* **438**, 763 (1995).
- ⁹N. E. L. Haugen and A. Brandenburg, "Suppression of small scale dynamo action by an imposed magnetic field," *Phys. Rev. E* **70**, 036408 (2004).
- ¹⁰A. Bershadskii and K. R. Sreenivasan, "Intermittency and the passive nature of the magnitude of the magnetic field," *Phys. Rev. Lett.* **93**, 064501 (2004).
- ¹¹O. Agullo, W.-C. Müller, B. Knaepen, and D. Carati, "Large eddy simulation of decaying magnetohydrodynamic turbulence with dynamic subgrid-modeling," *Phys. Plasmas* **8**, 3502 (2001).
- ¹²T. J. R. Hughes, L. Mazzei, and A. A. Oberai, "The multiscale formulation of large eddy simulation: Decay of homogeneous isotropic turbulence," *Phys. Fluids* **13**, 505 (2001).
- ¹³W.-C. Müller and D. Carati, "Large-eddy simulation of magnetohydrodynamic turbulence," *Comput. Phys. Commun.* **5**, 44 (2002).
- ¹⁴W.-C. Müller and D. Carati, "Dynamic gradient-diffusion subgrid models for incompressible magnetohydrodynamic turbulence," *Phys. Plasmas* **9**, 824 (2002).
- ¹⁵N. E. L. Haugen and A. Brandenburg, "Inertial range scaling in numerical turbulence with hyperviscosity," *Phys. Rev. E* **70**, 026405 (2004).
- ¹⁶W.-C. Müller and D. Biskamp, "Scaling properties of three-dimensional magnetohydrodynamic turbulence," *Phys. Rev. Lett.* **84**, 475 (2000).
- ¹⁷A. Brandenburg and G. R. Sarson, "The effect of hyperdiffusivity on turbulent dynamos with helicity," *Phys. Rev. Lett.* **88**, 055003 (2002).
- ¹⁸A. Brandenburg and K. Subramanian, "Astrophysical magnetic fields and nonlinear dynamo theory," *Phys. Rep.* **417**, 1 (2005).
- ¹⁹For this type of a weakly compressible simulation, we find that the energies of solenoidal and potential components of the flow have a ratio $E_{\text{pot}}/E_{\text{sol}} \approx 10^{-4} - 10^{-2}$ at most scales; only toward the Nyquist frequency does the ratio increase to about 0.1. It is thus reasonable to assume that compressibility is irrelevant for the results presented here.
- ²⁰G. Erlebacher, M. Y. Hussaini, C. G. Speziale, and T. A. Zang, "Toward the large-eddy simulation of compressible turbulent flows," *J. Fluid Mech.* **238**, 155 (1993).
- ²¹N. E. L. Haugen, A. Brandenburg, and A. J. Mee, "Mach number dependence of the onset of dynamo action," *Mon. Not. R. Astron. Soc.* **353**, 947 (2004).
- ²²Z.-S. She and E. Leveque, "Universal scaling laws in fully developed turbulence," *Phys. Rev. Lett.* **72**, 336 (1994).
- ²³P. A. Davidson, *Turbulence. An Introduction for Scientists and Engineers* (Oxford University Press, Oxford, 2004), Chap. 6.6.2.
- ²⁴G. Falkovich, "Bottleneck phenomenon in developed turbulence," *Phys. Fluids* **6**, 1411 (1994).
- ²⁵W. Dobler, N. E. L. Haugen, T. Yousef, and A. Brandenburg, "Bottleneck effect in three-dimensional turbulence simulations," *Phys. Rev. E* **68**, 026304 (2003).
- ²⁶A. A. Schekochihin, S. C. Cowley, S. F. Taylor, J. L. Maron, and J. C. McWilliams, "Simulations of the small scale turbulent dynamo," *Astrophys. J.* **612**, 276 (2004).
- ²⁷W.-C. Müller and R. Grappin, "The residual energy in freely decaying magnetohydrodynamic turbulence," *Plasma Phys. Controlled Fusion* **46**, B91 (2004).
- ²⁸W.-C. Müller and R. Grappin, "Spectral energy dynamics in magnetohydrodynamic turbulence," *Phys. Rev. Lett.* **95**, 114502 (2005).